

Modification of Pt/Co/Pt film properties by ion irradiation

K. A. Avchaciov, W. Ren, F. Djurabekova, and K. Nordlund

Department of Physics and Helsinki Institute of Physics, University of Helsinki, Helsinki 00014, Finland

I. Sveklo and A. Maziewski

Faculty of Physics, University of Białystok, Ciołkowskiego 1L 15-245 Białystok, Poland

(Received 3 June 2015; revised manuscript received 14 September 2015; published 30 September 2015)

We studied the structural modifications of a Pt/Co/Pt trilayer epitaxial film under Ga^+ 30-keV ion irradiation by means of classical molecular dynamics and Monte Carlo simulations. The semiclassical tight-binding second-moment approximation potential was adjusted to reproduce the enthalpies of formation, the lattice constants, and the order-disorder transition temperatures for Co-Pt alloys. We found that during irradiation, the sandwich-type Pt(fcc)/Co(hcp)/Pt(fcc) film structure underwent a transition to the new solid solution α -Co/Pt(fcc) phase. Our analysis of the short-range order indicates the formation, within a nanosecond time scale, of a homogeneous chemically disordered solution. The longer time-scale simulations employing a Monte Carlo algorithm demonstrated that the transition from the disordered phase to the ordered $L1_0$ and $L1_2$ phases was also possible but not significant for the changes in perpendicular magnetic anisotropy (PMA) observed experimentally. The strain analysis showed that the Co layer was under tensile strain in the lateral direction at the fluences of 1.5×10^{14} – 3.5×10^{14} ions cm^{-2} ; this range of fluences corresponds to the appearance of PMA. This strain was induced in the initially relaxed hcp Co layer due to its partial transformation to the fcc phase and to the influence of atomic layers with larger lattice constants at upper/lower interfaces.

DOI: [10.1103/PhysRevB.92.104109](https://doi.org/10.1103/PhysRevB.92.104109)

PACS number(s): 75.70.-i, 61.80.-x, 75.30.Gw, 61.43.Bn

I. INTRODUCTION

Ion irradiation has proven itself as a powerful tool for modifying properties of materials on the nanoscale [1]. These include multilayered (MLs) magnetic films, which are interesting for magnetic applications [2–4] due to perpendicular magnetic anisotropy (PMA). Particular regions in Co/Pt films can be modified to change the magnetization direction from perpendicular (out-of-plane) to in-plane [5–7] by different types of ions in the 20-keV–2-MeV energy range. Due to a strong dependence of PMA on magnetic layer thickness and interface roughness [8–10], it is evident that *degradation* of magnetic anisotropy arises from ion-beam mixing, which reduces in-plane strain and Co-Pt hybridization at the interfaces. However, the *appearance* of PMA in MLs after ion irradiation is less understood.

It was found that irradiation of in-plane magnetized Pt(5 nm)/Co(3.3 nm)/Pt(20 nm) epitaxial thin films by Ga^+ ions with 30-keV energy and a fluence of 2.5×10^{14} ions cm^{-2} led to the transition from in-plane magnetization to out-of-plane magnetization [11]. Such a transition can be explained, for instance, by the formation of ordered phases during the intermixing of the layers. The candidates among known Co-Pt phases [12] with high magnetic anisotropy are $L1_0$ -type $\text{Co}_{50}\text{Pt}_{50}$ [12], $L1_1$ -type $\text{Co}_{50}\text{Pt}_{50}$ [13], and $D0_{19}$ -type $\text{Co}_{75}\text{Pt}_{25}$ [14,15]. In addition, the presence of platelike Co clusters parallel to the sample surface in ordered $L1_2$ -type $\text{Co}_{25}\text{Pt}_{75}$ films may induce PMA as well [16,17]. All these lattices [except for the $D0_{19}$, which has a hexagonal close-packed (hcp) structure] are similar to a face-centered-cubic (fcc) structure and differ from equilibrium (α -Co, Pt) solid solutions [18] by chemical ordering and the c/a ratio. At the same time, the extended x-ray-absorption fine-structure (EXAFS) analysis of the irradiated films [19] showed significant in-plane tensile strain, which is quite opposite to the results [8] for similar

but thinner Pt(2.5 nm)/Co(1.3 nm)/Pt(3.7 nm) films irradiated by He^+ ions. A high lateral strain is typical for thin Co [20] and hcp-CoPt [21] films with thicknesses less than 1.5 nm in which PMA is present and strain appearance in the irradiated 3.3-nm-thick film could explain the observed PMA as well.

A vast variety of possible structures and strain effects along with the complication of experimental detection of chemical order in random mixed alloys confounds a clear understanding of the nature of PMA in irradiated Co/Pt thin films. In the present paper, we simulated the structural modifications of Pt-Co-Pt sandwich-type thin films caused by Ga^+ 30-keV ion irradiation by means of molecular dynamics (MD) and Monte Carlo (MC) methods. We focused on the analysis of the long-range order (LRO) and short-range order (SRO) in the simulated structures. We correlate the found structural modifications with anisotropic magnetic properties observed experimentally in these films to elucidate the nature of the induced PMA.

II. METHODS

In the present paper, the irradiation processes of Pt/Co/Pt thin films were simulated by using the PARCAS [22] and LAMMPS [23] codes which are based on the classical MD method. This method relies on interatomic potentials developed to describe atomic interactions resulting in macroscopically observable properties of the material of interest. This is the reason why we pay particular attention to the validity and applicability of the chosen interatomic potential to the problem at hand.

A. Potential development

Order-disorder transitions in Co-Pt alloys have been extensively studied by computer simulations over the past few

decades. The Ising model of ordering in Co-Pt alloys [24], for instance, demonstrated the importance of the contribution of pair exchange interactions dependent on magnetic states to the total energy of the system. Moreover, recent *ab initio* calculations [25,26] showed that chemical ordering is driven by magnetic interactions as well. The quantum-mechanical nature of magnetism puts in question the applicability of classical potentials to study the magnetic ordering in Co-Pt alloys. It was, however, pointed out [26] that the classical empirical potentials can, in principle, describe the right behavior of magnetic systems by including specific correction terms responsible for magnetic interactions. This idea is supported by various MC calculations of the order-disorder transition in Co-Pt alloys using classical potentials: the modified embedded-atom method (MEAM) [27,28] and tight-binding second-moment approximation (TB-SMA) [28–30]. These potentials were developed without a magnetic term, but it was assumed that the energy state of the ordered phases ($L1_0, L1_2$) is lower than that of the chemical disordered fcc phase ($A1$) and the energy difference correlates with the transition temperature T_t as $\Delta E \approx k_B T_t$, where k_B is the Boltzmann constant. We used a similar approach to develop an empirical potential suitable for both MD simulations of ion irradiation of Co/Pt thin films and the study of order-disorder transitions in these systems.

The TB-SMA model [31–33] was used as a functional form for energy expression. Here, the energy E_i of a particle with the index i is calculated as the sum of the attractive band energy E_i^b and the repulsive pair interaction E_i^r ,

$$E_i = E_i^b + E_i^r,$$

where

$$E_i^b = - \left\{ \sum_{j, r_{ij} < r_c} \xi_{IJ}^2 \exp \left[-2q_{IJ} \left(\frac{r_{ij}}{r_0^{IJ}} - 1 \right) \right] \right\}^{1/2}, \quad (1)$$

$$E_i^r = \sum_{j, r_{ij} < r_c} A_{IJ} \exp \left[-p_{IJ} \left(\frac{r_{ij}}{r_0^{IJ}} - 1 \right) \right]. \quad (2)$$

Here, the subscripts I and J refer to the type of atoms (Co or Pt), correspondingly, and the sums are taken over all atoms j within the cutoff distance r_c .

Initially we assumed the parameters A , ξ , p , q , r_0 , and r_c as in Ref. [34] where the pure components of the Co/Pt system were fitted to the experimental values of the cohesive energies, lattice constants, and bulk moduli, and the mixed system was described by adjusting the parameters to reproduce the correct value of the heat of dissolution in the dilute solution limit. We found, however, that the melting point of Co bulk was strongly underestimated, which caused too intense atomic mixing in high-energy atomic cascades during ion irradiation. To avoid this problem we used the parameters for Co-Co interactions as in Ref. [35], which resulted in a more accurate melting point for pure cobalt.

The remaining parameters (ξ_{IJ} , q_{IJ} , ξ_{JI} , q_{JI} , A_{IJ} , p_{IJ} , $r_{0,IJ}$, and $r_{c,IJ}$), which define the cross-species interactions, were readjusted. The reference values [18] included the enthalpies of formation ΔH^S and the lattice constants a, c for ordered and disordered phases of CoPt and CoPt₃ alloys.

TABLE I. TB-SMA model parameters used in Eqs. (1) and (2). The cutoff distances for Co-Co, Pt-Pt, and Co-Pt interactions are 5.0, 4.8, and 4.786 Å, respectively.

Parameters	ξ (eV)	q	A (eV)	p	r_0 (Å)
Pt-Pt [34]	2.506	3.680	0.242	11.140	2.77
Co-Co [35]	1.488	2.286	0.095	11.604	2.51
Pt-Co ^a	2.3223	3.7358	0.2515	17.344	2.556
Co-Pt ^a	2.2787	4.6478	0.2515	17.344	2.556

^aPresent paper.

Optimal parameters, found by solving the least-squares problem with the genetic algorithm [36], are presented in Table I. Values obtained with the new parametrization are shown in Table II and compared to existing TB-SMA potentials [30,34].

Additionally, we calculated the enthalpies of formation for several ordered Co-Pt alloys and compared them to ones for solid solutions with fcc and hcp lattices. As seen in Fig. 1, the most energetically favorable phases are chemically ordered, except for the $L1_1$ -CoPt phase, which has the lower ground state than the disordered phase according to *ab initio* calculations [25,26].

The Ga-Pt, Ga-Co, and Ga-Ga interactions were described as a repulsive Ziegler-Biersack-Littmark (ZBL) universal screening function [37], which was set smoothly to zero with a fifth-order polynomial at a distance from 4.5 to 4.8 Å. Additionally, the pair potential part E_{ij}^r was replaced by the ZBL function at short distances ($r_{ij} < 1.5$ Å) for a better description of the high-energy interactions of Pt-Pt, Co-Co, and Pt-Co.

B. Simulation setup

The Pt/Co/Pt sandwich-type thin film was constructed by joining three rectangular boxes containing bulk fcc Pt and bulk hcp Co. The boxes were stacked in the manner of a sandwich in the following order: (i) the 5-nm-thick Pt(111) top layer, (ii) the 3.3-nm-thick Co(0001) middle layer, and (iii) the 20-nm-thick Pt(111) bottom layer. The schematic of the simulation box is shown in Fig. 2.

TABLE II. Lattice constants and enthalpies of formation calculated with the new TB-SMA parametrization and the corresponding reference values taken from Ref. [18]. Values calculated with other TB-SMA parametrization sets [30,34] are presented for comparison.

	Fitted	Expt. [18]	TB-SMA [30,34]	
a_{A1}	Å	3.756	3.735	3.778, 3.771
a_{L1_0}	Å	3.793	3.793	3.898, 3.938
c_{L1_0}/a_{L1_0}		0.97	0.97	0.91, 0.88
$\Delta H_{L1_0}^S$	eV	0.242	0.141	0.200, 0.215
ΔH_{A1}^S	eV	0.146		0.144, 0.152
$T_{L1_0 \rightarrow A1}$	K	980	1098	700, 350 ^a
a_{L1_2}	Å	3.805	3.831	3.854, 3.849
$\Delta H_{L1_2}^S$	eV	0.164	0.126	0.122, 0.125
$T_{L1_2 \rightarrow A1}$	K	850	1023	350, 300

^aTransition from a fcc to a bcc structure.

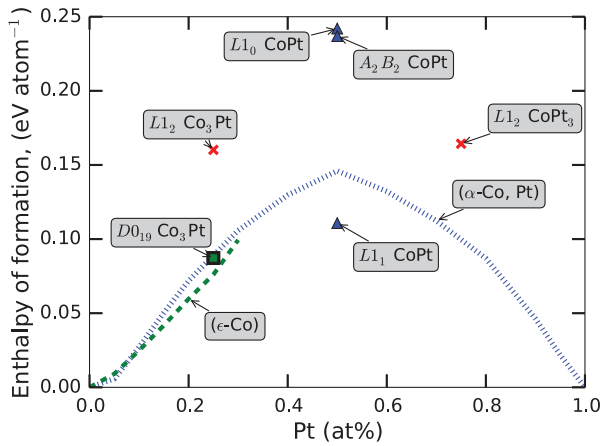


FIG. 1. (Color online) Enthalpies of formation ΔH^S obtained from the fitted potential for the solid solution of Co in the Pt fcc lattice (blue dotted line), solid solution of Pt in the Co hcp lattice (green dashed line), and various chemically ordered compositions marked in the figure.

The thicknesses of the layers were chosen to match exactly some of those used in recent experiments [11]. The lateral size of the simulation box was approximately

$20 \times 21 \text{ nm}^2$, and, due to the mismatch between the Pt and the Co lattice constants, the Pt and Co boxes had different numbers of unit cells on the xy plane. The box with Pt consisted of 48×44 cells, and the box with Co consisted of 40×49 cells. This resulted in 40 edge dislocations per interfacial area in total. The box contained 7.2×10^5 Pt atoms and 1.3×10^5 Co atoms. Periodic boundary conditions were used in x and y directions.

Additionally, we studied the dependence of initial strains in the modeled sandwich-type interfaces on the Co layer thickness. The initial configuration was similar to the one

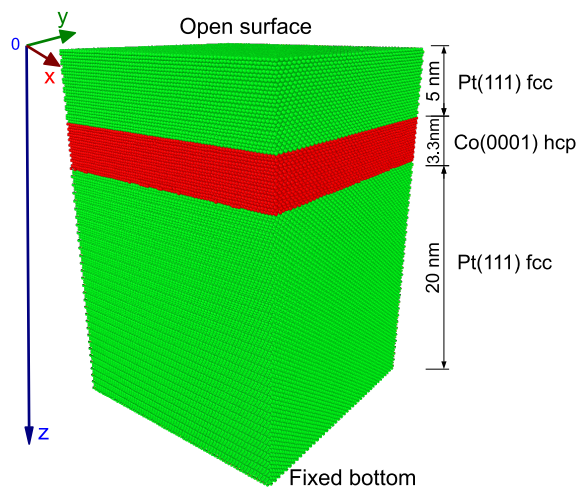


FIG. 2. (Color online) Three-dimensional visualization of the Pt/Co/Pt film after thermal relaxation: (i) 5-nm Pt(111) fcc top layer, (ii) 3.3-nm Co(0001) hcp middle layer, and (iii) 20-nm Pt(111) fcc bottom layer. The lateral size of the film is approximately $20 \times 20 \text{ nm}^2$. Pt and Co atoms are represented by green and red spheres, correspondingly.

described above, except for the thickness of the Co layer, which was varied in the range of 0.8–5.0 nm.

C. Molecular dynamics simulations of ion irradiation of Pt/Co/Pt thin films

Before simulations of ion irradiation, the simulation box was relaxed at room temperature using the Berendsen [38] temperature during 200 ps. During the ion irradiation runs the periodic boundary conditions were applied along the X and Y axes. The top surface was kept open, and three atomic layers were fixed at the bottom to prevent the entire system from moving during the bombardments. The incoming Ga^+ ions with the energy of 30 keV bombarded successively the open surface. The location of the subsequent impact was chosen at random by shifting randomly the cell in the lateral directions after the previous impact. All irradiation events were simulated at room temperature and with normal angles of incidence. We included electronic stopping as an additional force, which was applied on every atom with kinetic energy higher than 10 eV. Magnitude of the force was calculated from the data provided in the stopping and range of ions in matter (SRIM) [39] software according to the kinetic energy of the atom, and the force direction was opposite to the direction of the velocity vector of the atom. To model heat dissipation from the impact region, the Berendsen temperature scaling was applied at the periodic lateral boundaries with a layer thickness of 0.5 nm, which was immersed in the heat bath at 300 K. Each irradiation event was simulated during 120 ps, which was sufficiently long to cool the entire system to room temperature. The Ga atoms were removed from the sample after each impact. We neglected possible effects of the presence of Ga, such as the formation of the Ga-Pt or Ga-Co alloys and lattice distortions, due to its small concentration. The maximum Ga atomic concentration was lower than 1% at the highest fluence.

D. Monte Carlo simulations of the order-disorder transition

We studied the order-disorder transitions in the Pt/Co systems by performing the isothermal-isobaric (NPT) ensemble simulations with the coupled Metropolis MC and MD techniques as implemented in the LAMMPS [23] code. After the relaxation run performed by MD, we applied the MC swapping step between Co and Pt atoms. Two atoms for a swap were selected randomly with equal probability among all the atoms and were always of different types. The swap of the selected atoms was accepted with respect to the change in the potential energy of the system ΔE at the fixed temperature after the swap ($\Delta E = E_a - E_b$, where E_b and E_a are the total energies of the system before and after the swap) in accord with the Metropolis criterion: Either $\Delta E < 0$ and thus the configuration after the swap was more favorable, or the factor $\exp(-\Delta E/k_B T)$ was less than a random number uniformly generated in $[0,1]$. Between the two subsequent MC swapping steps ten MD steps were performed, and this procedure was repeated until the system reached the thermal equilibrium.

The described MC algorithm was modified to study the order-disorder transitions in the irradiated structures. Since the atomic concentrations of Co and Pt were not homogeneous in the entire simulation cell, the swaps between two randomly

chosen atoms from anywhere in the cell would lead to enhanced atomic mixing and smoothening of the distributions of atoms of different species through the cell. Although this may happen on very long time scales, since both metals are miscible, we aim to analyze the atomic composition of the irradiated cells within finite time scales. Thus, we limited the environment for the choice of the two atoms for a swap to the first-nearest neighbors only. This modification is motivated by the mechanism of self-diffusion via atom-vacancy exchange, which is limited to the bond length [40]. In this approach, we assumed that the concentration of vacancies is nonequilibrium and due to many successive cascades is sufficient for the swap candidates to be chosen with equal probability among all atoms.

E. Analysis methods

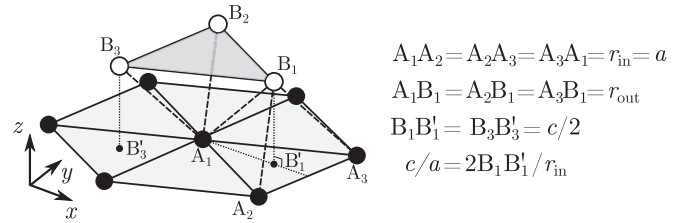
We performed an analysis of the chemical SRO (CSRO), LRO, interface roughness, and strains in the irradiated samples, which were preliminarily quenched at 0 K using the conjugate gradient algorithm. For the strain analysis, we removed the periodic boundary condition in the x and y directions resulting in the formation of additional open surfaces. This allowed relaxation of lateral strains in the layers of Pt and Co separate from each other. We excluded the contribution from the surface tension and defects caused due to the breakage of periodicity by not taking into account atoms in the subsurface regions. The cutoff distance of 1.5 nm was used to define the subsurface regions (both for the top and for the side surfaces).

The CSRO was characterized by the short-range order parameter (SROP). The SROP was calculated as the ratio of the number of chemically ordered atoms to the total number of atoms in the system. Here, we defined the local chemical order in terms of chemical bond arrangement for the atoms up to the second-nearest-neighbor environment.

In our simulation cells, we defined the $L1_0$ and $L1_2$ phases as follows. An atom i of type I was considered to have the $L1_0$ order if the next requirements were fulfilled: (i) It had 12 nearest neighbors; (ii) eight of them were of type J and the four remaining were of the same type I ; (iii) the bonds between atom i of type I and its four I -type neighbors belonged to the same plane. The normal vector to this plane defined the orientation of the $L1_0$ unit cell and corresponded to the easy axis of magnetization. An atom i of type I was defined as having the $L1_2$ order, if: (i) It had 12 nearest and six second-nearest neighbors; (ii) 12 nearest-neighbor atoms were of type J ; (iii) five or six second-nearest neighbors were of type I .

The LRO was characterized by the lattice structure type. There were two possible types of the lattice: fcc [preferred for pure Pt and (α -Co,Pt) solid solutions] and hcp (pure Co). The lattice type was analyzed with the adaptive common neighbor analysis (a-CNA) method [41,42] implemented in the OVITO package [43]. Atoms with fcc lattices were indexed by 1, and atoms with hcp lattices were indexed by 2.

Interface roughness was measured in two steps: First, the mathematical models of the surfaces representing the top part of the upper Pt layer, the upper Pt-Co interface, and the lower Co-Pt interface were produced with a polyhedral mesh [44]; second, the standard deviation of the Z coordinate from every mesh element was calculated and defined as roughness.



$$\begin{aligned} A_1A_2 &= A_2A_3 = A_3A_1 = r_{\text{in}} = a \\ A_1B_1 &= A_2B_1 = A_3B_1 = r_{\text{out}} \\ B_1B_1' &= B_3B_3' = c/2 \\ c/a &= 2B_1B_1'/r_{\text{in}} \end{aligned}$$

FIG. 3. Schematic of two packing layers in the hcp lattice. The points A_1 , A_2 , A_3 , and B_1 form a triangular pyramid with the triangular base $A_1A_2A_3$ and with the height B_1B_1' . The c/a ratio is equal to $2B_1B_1'/A_1A_2$, where $B_1B_1' = \sqrt{r_{\text{out}}^2 - r_{\text{in}}^2/3}$.

To analyze the strain induced by ion irradiation, we calculated the average length of the Co-Co bonds along the z axis. We separated the Co-Co bonds into in-plane bonds and out-of-plane bonds according to their packing. Lengths of the in-plane bonds (r_{in}) were calculated for atoms belonging to the same close-packed plane as shown in Fig. 3. Lengths of the out-of-plane bonds (r_{out}) were calculated for atoms on neighboring close-packed planes (see Fig. 3). We characterize lateral strain in the hcp matrix with the c/a ratio. In the perfect hcp structure with the c axis directed along the z axis, the c/a ratio is expressed as follows:

$$c/a = 2 \frac{\sqrt{r_{\text{out}}^2 - r_{\text{in}}^2/3}}{r_{\text{in}}}. \quad (3)$$

The c/a ratio in the irradiated samples was calculated using Eq. (3). The direction of the c axis coincided with the direction of the z axis since the Co-rich layer retained an initial (0001) orientation of hcp Co and no grains of different crystallographic orientations formed during irradiation.

III. RESULTS AND DISCUSSION

A. Simulation of order-disorder transition in bulk Co/Pt alloys

With the purpose to verify that the fitted values for enthalpy of formation (Table II) correspond to the target transition temperatures, we applied the MC swapping algorithm to simulate order-disorder transitions in bulk Co/Pt alloys. The simulation cell containing 4000 atoms was constructed from ordered and disordered phases in proportion 1:1. It was initially relaxed in MD runs for 10 ps in the NPT ensemble for various temperatures and zero pressure. We performed a series of the runs in the range of temperatures of 500–1100 K with the increment of $\Delta T = 50$ K. The results are shown in Fig. 4 where the SROP value was averaged over 20 frames taken every 10 ps after the thermal equilibration had been obtained. The estimated temperature of the $L1_0 \rightarrow A1$ transition was 980 K for the CoPt alloy and the $L1_2 \rightarrow A1$ transition was 850 K for the CoPt₃ alloy. As shown in Table II, the calculated transition temperatures are underestimated for the CoPt₃ alloy by 170 K and for the CoPt alloy by 120 K in comparison to the experimental values. It was found that the MC algorithm with a MD relaxation step in an NPT ensemble predicted a phase transition at lower temperatures compared to the values reported [27,30] for the MC simulations for a canonical ensemble without MD relaxation. This effect can be attributed

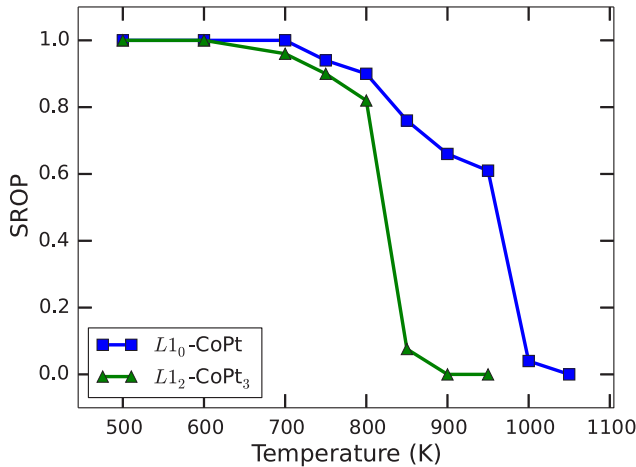


FIG. 4. (Color online) Temperature dependence of SROP for ordered L_{10} -CoPt and L_{12} -CoPt₃ alloys in coupled MC/MD simulations. The L_{10} -CoPt phase reaches disorder state A1 at 1050 K and L_{12} CoPt₃ at 950 K. The transition temperature is estimated as the temperature where the SROP equals 0.5.

to thermal expansion of the sample in NPT simulations as well as to the more effective lattice relaxation due to atomic displacements along the force vector in MD [45].

B. MD simulations of ion irradiation of Pt/Co/Pt thin films

1. Mixing and long-range ordering

The irradiation simulations were run for 2000 consistent impacts in total. From all these impacts we chose four for detailed analysis, which correspond to the cases of different reorientations of magnetization observed in the experiments [11]. At the very low fluence of 1.0×10^{14} ions cm^{-2} (420 impacts) the film retained its initial in-plane magnetization. Starting from this fluence, the reorientation of magnetization from the in-plane to the out-of-plane direction occurred, and the maximum of the magnetic anisotropy was observed at the fluence of 2.5×10^{14} ions cm^{-2} (1045 impacts). With further dose accumulation, the reorientation of magnetization took place in the opposite way: from the out-of-plane to the in-plane direction. We chose the intermediate configuration at the fluence of 3.5×10^{14} ions cm^{-2} (1460 impacts) to characterize this regime. Finally, magnetization turned to in plane at fluences higher than 4.2×10^{14} ions cm^{-2} (1760 impacts).

The depth profiles of Co atomic concentration from our MD simulations are shown in Fig. 5. In addition, the same profiles, but obtained with the binary collision approximation code TRIDYN [46] are given for comparison. According to the calculated profiles, the equiatomic composition required for formation of the ordered L_{10} -CoPt phase could be found near the upper interface at the depth between 4 and 5 nm and near the lower interface at the depth between 8 and 9 nm. The L_{12} CoPt₃ could be formed at the same depths as the L_{10} phase, whereas L_{12} Co₃Pt is expected to grow inside the Co layer at depths between 5 to 6 nm and 7.3–8.3 nm.

Both MD and TRIDYN profiles have asymmetric shapes with the bias towards the surface, which indicates a stronger

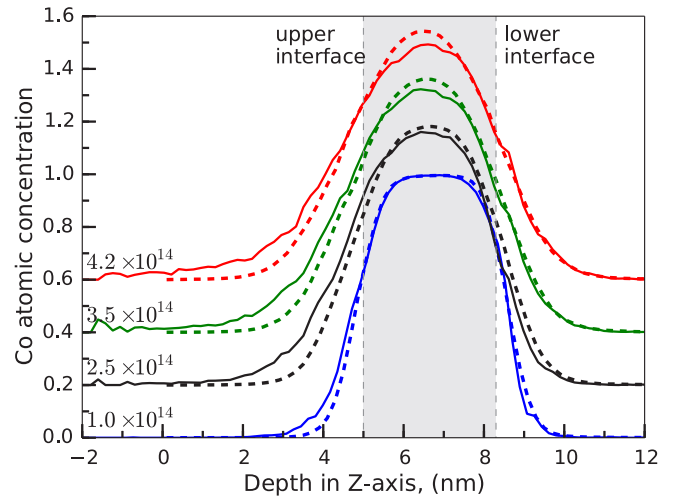


FIG. 5. (Color online) Depth profiles of Co atomic concentration of the irradiated system at the fluences of 1.0×10^{14} , 2.5×10^{14} , 3.5×10^{14} , and 4.2×10^{14} ions cm^{-2} by MD simulations (solid lines) and TRIDYN simulations (dashed lines). Curves with different fluences are shifted by 0.2 from each other. The filled gray area corresponds to the initial position of the Co layer.

intermixing of Co and Pt at the upper interface and can be explained by the asymmetric distribution of vacancies with respect to the Co layer (see Fig. 6). The bias is more significant for profiles obtained in MD simulations and increases with an accumulated dose. This distinction is explained by different cascade relaxation effects in both MD and TRIDYN, which becomes more pronounced in the presence of the surface. The dense collision cascades form the thermal spikes (molten) regions in MD simulations, which recrystallize much faster in the bulk than in the surface layers due to the different efficiencies of heat dissipation [47], which, as a result, lead to a stronger atom mixing near the surface. However, the effect of thermal spikes is less noticeable at depths far from the surface where the MD and TRIDYN profiles are similar to each other. The low influence of thermal spikes on mixing is typical for metals with high melting temperatures [48], such as Pt.

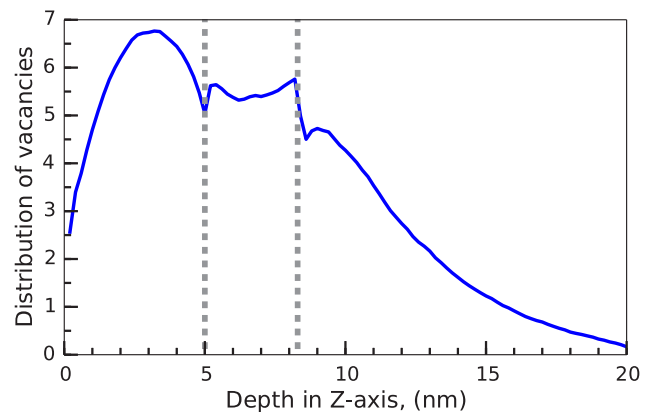


FIG. 6. (Color online) Distribution of vacancies in the studied structure as obtained by SRIM [39]. The dashed lines indicate the Pt/Co interfaces. The larger number of vacancies near the upper interface enhances the Co/Pt intermixing.

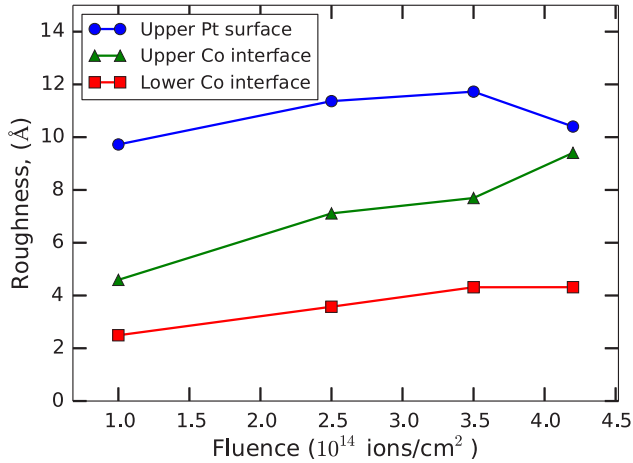


FIG. 7. (Color online) Surface/interface roughness calculated for the top surface of the Pt layer (circles), the upper Co interface (triangles), and the lower Co interface (squares).

The difference between upper and lower interfaces is clearly seen in Fig. 7 where the surface and interface roughnesses are presented as a function of the fluence. The roughness of the upper Co interface was found to be much higher than the roughness of the lower Co interface. This result correlates very well with the measurements of interface roughness by x-ray reflectometry [8] where the roughness was found to be more pronounced near the upper Co/Pt interface compared to the lower one. Also, we note that the surface (top Pt layer) becomes fairly rough already at low fluences, visible in the shape of craters. Such surface roughening is typical for collision cascades in the heat spike regime due to the plastic flow of atoms and cratering [49–52]. With the increase in the fluence, the roughness of the Pt surface is not increasing much due to crater annihilation [53,54] during subsequent impacts.

The CNA analysis (Sec. II E) showed that the structure remained crystalline with a negligible fraction of point defects, dislocations, and stacking faults after irradiation at all fluences. In Fig. 8 we presented the type of lattice structure as a function of depth. Here, we excluded atoms with an undefined lattice type, which were interstitials, vacancies, and the surface atoms. Stacking faults and dislocation, however, are taken into account in the analysis shown in Fig. 8 and contribute to the peaks at depths of 3–5 and 8–10 nm. The pronounced peaks at depths of -2 to 1 nm are caused by changes in the surface morphology due to its high roughness. We observed that transformation from the fcc to the hcp structure occurred with a couple of the upper atomic layers on the surface protrusions. As the most significant result, we found that the thickness of the hcp Co layer was changing with the fluence. From the initial value of 3.3 nm in the as-prepared sample, the thicknesses were reduced to 2, 1, and 0.5 nm at the fluences of 1.0×10^{14} , 2.5×10^{14} , and 3.5×10^{14} ions cm⁻², correspondingly. The hcp structure vanished completely at the fluence of 4.2×10^{14} ions cm⁻². This result indicates that during irradiation, the transition from the ϵ -Co/Pt hcp phase to the α -Co/Pt fcc phase occurs at both the upper and the lower interfaces. Assuming the strong dependence of magnetic anisotropy on the thickness of the Co layer in trilayer Pt/Co/Pt

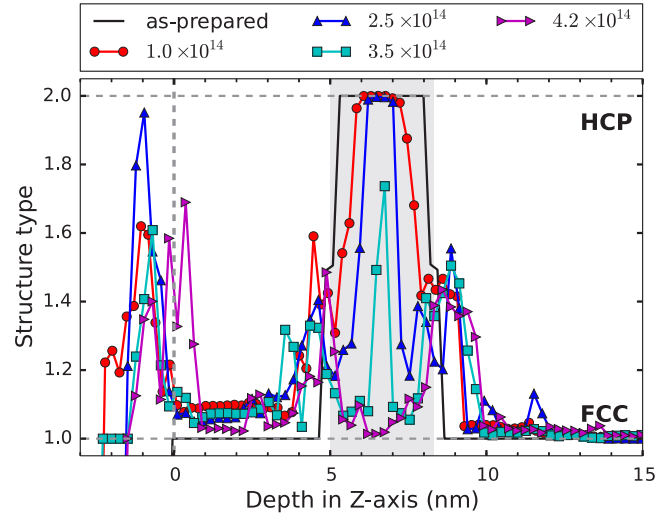


FIG. 8. (Color online) Lattice type calculated with CNA as a function of depth. Atomic layers with perfect fcc lattices have values of 1, whereas layers with perfect hcp lattices have values of 2. Layers with noninteger values contain the mixture of fcc and hcp structures, which is typical for stacking faults. The filled gray area denotes the initial position of the Co layer.

films [11], this variation in the thickness of the hcp layer could already explain the appearance of PMA. However, according to *ab initio* studies [55], the appearance of PMA in hcp Co is related to a lateral tensile strain and the reduction in the c/a ratio, which was experimentally observed [21] only in the thin hcp Co/Pt structures. We also performed the calculation of strains in the irradiated samples, which will be addressed later on in the discussion.

2. Short-range ordering

The SRO analysis of the configurations obtained in the MD simulations did not exhibit any significant chemical ordering, except for a few single atoms in the $L1_0$ or $L1_2$ phases, which may be also attributed to random fluctuations. This observation is in agreement with previous works [56,57] on disordering kinetics in irradiated intermetallic compounds. It was found that degradation of chemical SRO occurs in chemically ordered alloys in the collisional cascades due to the different time scales of the LRO and the chemical SRO recovery process. Thus, a crystalline structure restores quickly, preventing the chemical ordering; this happens in molten zones due to enhanced mobility of atoms. In our case of the trilayer film with no initial chemical SRO, the appearance of the latter during the cascade quenching is highly unlikely. Also, the time scale, which can be reached in MD simulations for the postcascade relaxation process, is several orders of magnitude lower than that predicted in MC simulations [58,59] of chemical ordering induced by displacement cascades. The distortion of chemical SRO is recovered by the vacancy migration mechanism at times on the order of tens of milliseconds. Taking into consideration all these limitations, we performed the structure optimization simulations of the MD-simulated irradiated films with the coupled MD-MC technique.

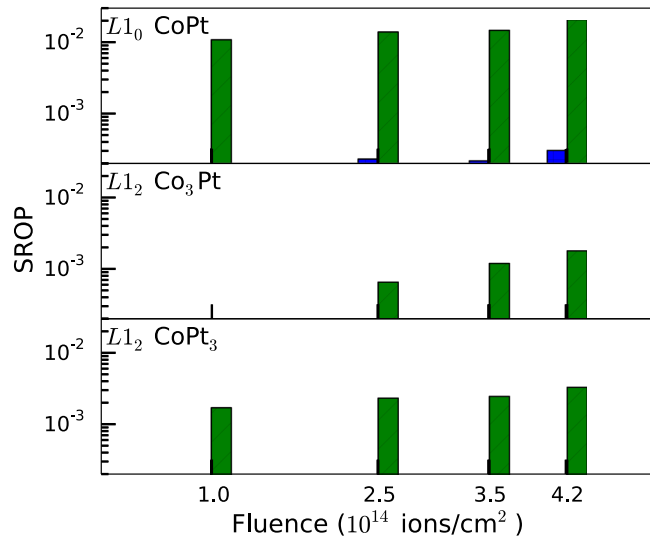


FIG. 9. (Color online) Short-range order parameter calculated for L_{10} and L_{12} phases before (blue bars) and after (green bars) MD-MC optimization.

We studied four configurations obtained in MD simulations discussed above at the fluences: 1.0×10^{14} , 2.5×10^{14} , 3.5×10^{14} , and 4.2×10^{14} ions cm^{-2} . Simulations were performed at room temperature and zero pressure for 10^6 MD steps and 10^7 MC steps. The number of simulation steps was sufficient to obtain stable fractions of the ordered phases although low enough to prevent homogenization of the system. After that the chemical SRO analysis was performed for all structures and the SROP was calculated. As the normalization factor, we chose the number of atoms in the region with nonzero Co atomic concentration, which was approximately equal to 3×10^5 for all fluences. In Fig. 9 we present the bar diagrams where the SROP is shown separately for L_{10} CoPt, L_{12} Co_3Pt , and L_{12} CoPt_3 . We found the presence of both L_{10} and L_{12} ordered phases, which were not observed in MD simulations, but were predicted from the depth profiles of atomic concentrations in Sec. III B 1. The fraction of the magnetically anisotropic L_{10} phase monotonically grows with the fluence as seen in Fig. 9. It happens due to mixing of the Co and Pt layers as the fluence increases. It can be seen in Fig. 5 that atomic concentration profiles become wider with the fluence, and hence the regions where the equiatomic composition of Co and Pt can be observed are enlarging. The appearance of PMA at low fluences could be explained by the growth of the L_{10} phase. However, our results cannot explain the disappearance of PMA at high fluences as the L_{10} phase continues to grow. Thus, the origin of induced magnetic anisotropy is not related to the formation of the ordered L_{10} phase.

3. Strains

We analyzed strains in the irradiated samples, which were not optimized with the MD-MC technique. As the presence of the L_{10} phase does not correlate with the observed magnetic properties, we did not find it necessary to analyze strains in the structures obtained after the MD-MC optimization. The results are shown in Fig. (a) It can be seen that both bond lengths,

in-plane and out-of-plane, increase with the distance from the initial position of the Co layer where the atomic concentration of Pt becomes higher. Taking into account the facts that Co atoms are incorporated in the fcc matrix and that the lattice constant in the α -Co/Pt alloy grows with Pt concentration, we assume that the increase in the Co-Co distance is due to the Co-Pt alloying rather than to the induced strain. Also, the same length of in-plane bonds and out-of-plane bonds does not allow for distinction between different crystallographic directions and, thus, should not cause the appearance of PMA.

Inside the Co layer, we observed the difference between in-plane and out-of-plane bonds, which is typical for hcp crystals with a nonideal axial ratio (c/a). However, this difference vanished at the upper Pt/Co and lower Co/Pt interfaces, indicating the transition from the hcp to the fcc structure. At the fluences of 3.5×10^{14} and 4.2×10^{14} ions cm^{-2} , the difference between orientations is almost indistinguishable. Both in-plane and out-of-plane bond lengths grow with the fluence due to the penetration of Pt atoms inside the hcp matrix; however, as it was shown later, this effect depends not only on Pt concentration, but also on a thickness of the hcp layer. In Fig. 10(b) we plot the c/a ratio. The equilibrium c/a ratio calculated for bulk hcp Co was 1.615; however, in the as-prepared epitaxial films it was lower and amounted to 1.604. At the fluence of 1.0×10^{14} ions cm^{-2} the calculated c/a ratio was about the same as for as-prepared sample, and at the fluence of 2.5×10^{14} ions cm^{-2} it decreased, which points to the presence of lateral tension inside the Co layer. With a further increase in the fluence, the c/a ratio grew up towards the ideal ratio of 1.633 typical for the fcc structure. The decrease in the c/a ratio at 2.5×10^{14} ions cm^{-2} could not be explained by the chemical composition of the ϵ -Co/Pt hcp phase; as in the bulk sample, this ratio stays constant with increasing Pt atomic concentration. The decreased value of the c/a ratio indicates the presence of strain inside the hcp layer due to its thinning, whereas interface atoms are at the influence of upper/bottom layers with larger lattice constants. This idea correlates with the CNA analysis discussed in Sec. III B 1. Thus, in the nonirradiated sample and in the sample at the fluence of 1.0×10^{14} ions cm^{-2} , the thickness of the hcp layer is higher than the critical value at which strains are present. Although the transition from the hcp to the fcc structure occurs in the interfaces during ion-beam mixing, the hcp layer becomes thinner, and the strain in it is increased.

To prove this hypothesis, we studied the strain distribution in the Pt(5 nm)/Co(d_{Co})/Pt(20 nm) films by varying the thickness of the Co layer. In Fig. 11 we plot the bond lengths for in-plane and out-of-plane directions along with the c/a ratio inside of the Co layer. For the thickness of $d_{\text{Co}} > 2$ nm, the bond lengths and c/a do not change with increasing layer thickness. The c/a ratio is lower than the bulk value, which indicates the presence of tensile strain inside of the Co layer. However, the values obtained from the experimental measurements [20,21] for the same Co thickness match the c/a ratio in the unstrained bulk Co. We assume that the initial strain observed in MD in the thick (> 2 -nm) layers is related to the imperfection of the interatomic potential and to the idealized model of the as-prepared interface with zero roughness, which

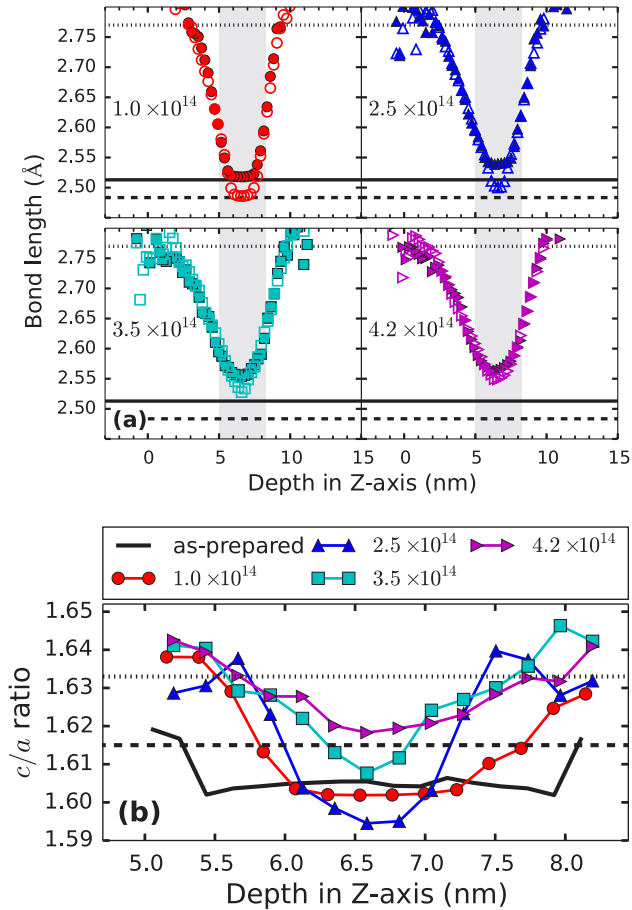


FIG. 10. (Color online) (a) Average length of the Co-Co bond lying inside the *xy* plane (filled markers) and outside the *xy* plane (unfilled markers) as a function of depth. The horizontal solid and dashed lines point to the average values for in-plane and out-of-plane bonds, correspondingly, in the as-prepared sample. The horizontal dotted line corresponds to the value of the Pt-Pt bond length in the as-prepared sample. (b) *c/a* ratio calculated at the depth of the Co layer at different fluences. The horizontal dashed and dotted lines indicate the values for the *c/a* ratio in bulk (unstrained) Co and Pt, correspondingly.

cannot be achieved in real structures. Nevertheless, as the *c/a* ratio stays constant at thicknesses of $d_{\text{Co}} > 2$ nm, it can be taken as the reference value. When the thickness of the Co layer decreases below 2 nm, both in-plane and out-of-plane bonds stretch, and the *c/a* ratio decreases due to the higher stretching in the lateral direction. Such dependence of the *c/a* ratio on the thickness is in agreement with experimental observations [20,21], see Fig. 11. Despite the difference in absolute values of the *c/a* ratios between calculations and experimental measurements, the identical trend in the increase in the *c/a* ratios with the Co layer thickness justifies the consideration of strain effect in MD simulations.

Comparing the values of bond lengths and the *c/a* ratio in the sample at the fluence of 2.5×10^{14} ions/cm² with the values obtained for perfect sandwich-type thin-film structures, we found that the irradiated sample is identical to the case of the perfect film with $d_{\text{Co}} = 0.8$ nm. This d_{Co} value matches

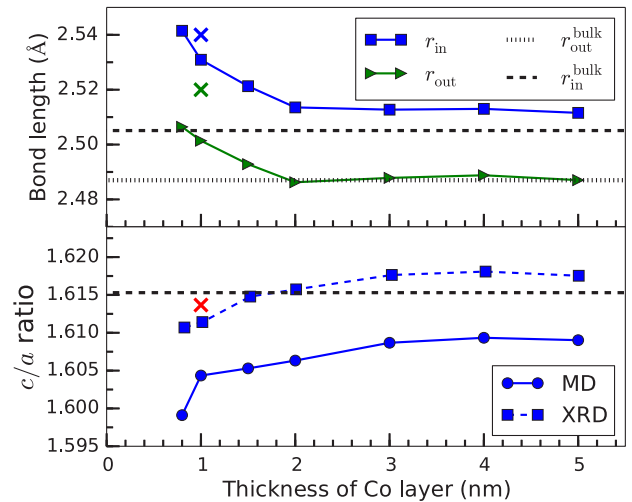


FIG. 11. (Color online) Co-Co bond lengths and *c/a* ratio as a function of Co layer thickness d_{Co} in trilayer films Pt(5 nm)/Co(d_{Co})/Pt(20 nm) calculated in the MD simulation (solid curves). Values of the *c/a* ratio (dashed curve) measured with x-ray diffraction (XRD) [21] in similar trilayer films are presented for comparison. The cross markers are values measured with EXAFS in the Pt(3.5 nm)/Co(1 nm)/Pt film [20]. The horizontal lines indicate the calculated values in unstrained bulk Co.

our estimations from the CNA analysis (Sec. III B 1) as the hcp layer inside the Co film has the same thickness.

We can conclude that by means of ion irradiation, the thickness of the hcp Co layer in the sandwich-type Pt/Co/Pt films can be tuned. This is possible by the alloying of Co and Pt layers in the interfaces promoted by collision cascades. Below a critical size of the hcp layer, the strain inside of the layer is present, which causes reorientation of magnetization from the in-plane to the out-of-plane direction.

IV. CONCLUSIONS

In the present paper, we carried out molecular dynamics simulations of irradiation of Pt/Co/Pt thin films to elucidate the nature of perpendicular magnetic anisotropy observed in recent experiments. The structural modifications caused by radiation in the studied system were analyzed with respect to the possible appearance of magnetic anisotropy. According to molecular dynamics simulations, irradiation of Pt/Co/Pt layered films with Ga⁺ ions causes ion-beam mixing of Co and Pt layers. Although the fcc long-range order was preserved in the irradiated structures, the molecular dynamics simulations could not capture a specific chemical short-range order, which could be associated with the possible magnetic anisotropy. Additional hybrid MC-MD simulations revealed the formation of only insignificant fractions of chemically ordered $L1_0$ -CoPt, $L1_2$ -Co₃Pt, and $L1_2$ -CoPt₃ phases, which occurred at the depths where atomic concentration of Co and Pt atoms matched the composition stoichiometry. Moreover, uniform growth of the ordered phases with the ion fluence does not correlate with the reported behavior of PMA.

On the basis of the strain analysis in the irradiated structures we suggest that the reorientation of magnetization can be

related to the strain induced inside of the Co layer. The tensile strain appears in the initially relaxed hcp layer during its gradual thinning. Thinning of the hcp layer is caused by the alloying

of two metals at the interfaces and formation of the α -Co/Pt fcc phase. The dependence of the hcp layer thickness on the ion fluence is in agreement with the behavior of the PMA.

-
- [1] A. V. Krashennnikov and K. Nordlund, Ion and electron irradiation-induced effects in nanostructured materials, *J. Appl. Phys.* **107**, 071301 (2010).
- [2] H. J. Richter, The transition from longitudinal to perpendicular recording, *J. Phys. D: Appl. Phys.* **40**, R149 (2007).
- [3] S. Mangin, D. Ravelosona, J. A. Katine, M. J. Carey, B. D. Terris, and E. E. Fullerton, Current-induced magnetization reversal in nanopillars with perpendicular anisotropy, *Nature Mater* **5**, 210 (2006).
- [4] A. Maziewski, J. Fassbender, J. Kisielewski, M. Kisielewski, Z. Kurant, P. Mazalski, F. Stobiecki, A. Stupakiewicz, I. Sveklo, M. Tekielak, A. Wawro, and V. Zablotskii, Magnetization states and magnetization processes in nanostructures: From a single layer to multilayers, *Phys. Status Solidi A* **211**, 1005 (2014).
- [5] G. J. Kusinski, K. M. Krishnan, G. Denbeaux, G. Thomas, B. D. Terris, and D. Weller, Magnetic imaging of ion-irradiation patterned Co/Pt multilayers using complementary electron and photon probes, *Appl. Phys. Lett.* **79**, 2211 (2001).
- [6] C. Vieu, J. Gierak, H. Launois, T. Aign, P. Meyer, J. P. Jamet, J. Ferr, C. Chappert, T. Devolder, V. Mathet, and H. Bernas, Modifications of magnetic properties of Pt/Co/Pt thin layers by focused gallium ion beam irradiation, *J. Appl. Phys.* **91**, 3103 (2002).
- [7] C. T. Rettner, S. Anders, J. E. E. Baglin, T. Thomson, and B. D. Terris, Characterization of the magnetic modification of Co/Pt multilayer films by He⁺, Ar⁺, and Ga⁺ ion irradiation, *Appl. Phys. Lett.* **80**, 279 (2002).
- [8] T. Devolder, Light ion irradiation of Co/Pt systems: Structural origin of the decrease in magnetic anisotropy, *Phys. Rev. B* **62**, 5794 (2000).
- [9] M. Kisielewski, A. Maziewski, M. Tekielak, A. Wawro, and L. T. Baczewski, New Possibilities for Tuning Ultrathin Cobalt Film Magnetic Properties by a Noble Metal Overlayer, *Phys. Rev. Lett.* **89**, 087203 (2002).
- [10] O. Robach, C. Quiros, P. Steadman, K. F. Peters, E. Lundgren, J. Alvarez, H. Isern, and S. Ferrer, Magnetic anisotropy of ultrathin cobalt films on Pt(111) investigated with x-ray diffraction: Effect of atomic mixing at the interface, *Phys. Rev. B* **65**, 054423 (2002).
- [11] A. Maziewski, P. Mazalski, Z. Kurant, M. O. Liedke, J. McCord, J. Fassbender, J. Ferré, A. Mougin, A. Wawro, L. T. Baczewski, A. Rogalev, F. Wilhelm, and T. Gemming, Tailoring of magnetism in Pt/Co/Pt ultrathin films by ion irradiation, *Phys. Rev. B* **85**, 054427 (2012).
- [12] D. Weller, A. Moser, L. Folks, M. E. Best, W. Lee, M. F. Toney, M. Schwickert, J.-U. Thiele, and M. F. Doerner, High Ku materials approach to 100 Gbits/in², *IEEE Trans. Magn.* **36**, 10 (2000).
- [13] H. Sato, T. Shimatsu, Y. Okazaki, H. Muraoka, H. Aoi, S. Okamoto, and O. Kitakami, Fabrication of L11 type Co-Pt ordered alloy films by sputter deposition, *J. Appl. Phys.* **103**, 07E114 (2008).
- [14] G. R. Harp, D. Weller, T. A. Rabedeau, R. F. C. Farrow, and M. F. Toney, Magneto-Optical Kerr Spectroscopy of a New Chemically Ordered Alloy: Co₃Pt, *Phys. Rev. Lett.* **71**, 2493 (1993).
- [15] Y. Yamada, W. P. Van Drent, T. Suzuki, and E. N. Abarra, On high magnetic anisotropy ordered phase Co₃ Pt alloy films with high magneto-optical Kerr activity, *J. Magn. Soc. Jpn.* **22**, 81 (1998).
- [16] M. Maret, M. Cadeville, R. Poinso, A. Herr, E. Beaupaire, and C. Monier, Structural order related to the magnetic anisotropy in epitaxial (111) CoPt₃ alloy films, *J. Magn. Magn. Mater.* **166**, 45 (1997).
- [17] C. Meneghini, M. Maret, V. Parasote, M. Cadeville, J. Hazemann, R. Cortes, and S. Colonna, Structural origin of magnetic anisotropy in Co-Pt alloy films probed by polarized XAFS, *Eur. Phys. J. B* **7**, 347 (1999).
- [18] B. Predel, in *Ca-Cd-Co-Zr*, edited by O. Madelung, Landolt-Börnstein, Physical Chemistry, Group IV, Vol. 5c (Springer, Berlin/Heidelberg, 1993).
- [19] M. Sakamaki, K. Amemiya, M. O. Liedke, J. Fassbender, P. Mazalski, I. Sveklo, and A. Maziewski, Perpendicular magnetic anisotropy in a Pt/Co/Pt ultrathin film arising from a lattice distortion induced by ion irradiation, *Phys. Rev. B* **86**, 024418 (2012).
- [20] J. Thiele, R. Belkhou, H. Bulou, O. Heckmann, H. Magnan, P. L. Fvre, D. Chandresris, and C. Guillot, EXAFS study of the crystallographic structure of cobalt thin films on Pt(111), *Surf. Sci.* **384**, 120 (1997).
- [21] T. Shimatsu, Y. Okazaki, H. Sato, O. Kitakami, S. Okamoto, H. Aoi, H. Muraoka, and Y. Nakamura, Large uniaxial magnetic anisotropy of Co-Pt perpendicular films induced by lattice deformation, *IEEE Trans. Magn.* **43**, 2995 (2007).
- [22] K. Nordlund (2010). PARCAS computer code. The main principles of the molecular dynamics algorithms are presented in Refs. [60,61]. The adaptive time step and electronic stopping algorithms are the same as in Ref. [62].
- [23] S. Plimpton, Fast parallel algorithms for short-range molecular dynamics, *J. Comput. Phys.* **117**, 1 (1995).
- [24] J. M. Sanchez, J. L. Moran-Lopez, C. Leroux, and M. C. Cadeville, Magnetic properties and chemical ordering in Co-Pt, *J. Phys.: Condens. Matter* **1**, 491 (1989).
- [25] A. Dannenberg, M. E. Gruner, A. Hucht, and P. Entel, Surface energies of stoichiometric FePt and CoPt alloys and their implications for nanoparticle morphologies, *Phys. Rev. B* **80**, 245438 (2009).
- [26] S. Karoui, H. Amara, B. Legrand, and F. Ducastelle, Magnetism: the driving force of order in CoPt, a first-principles study, *J. Phys.: Condens. Matter* **25**, 056005 (2013).
- [27] S. I. Park, B.-J. Lee, and H. M. Lee, Estimation of order-disorder transition temperature in Pt-Co alloy by Monte Carlo simulation using modified embedded atom method, *Scr. Mater.* **45**, 495 (2001).
- [28] P. Moskovkin and M. Hou, Metropolis Monte Carlo predictions of free Co-Pt nanoclusters, *J. Alloys Compd.* **434**, 550 (2007).
- [29] M. Allalen, H. Bouzar, and T. Mehaddene, Saddle-point energies and Monte Carlo simulation of the long-range order relaxation in CoPt, *Eur. Phys. J. B* **45**, 443 (2005).

- [30] G. Rossi, R. Ferrando, and C. Mottet, Structure and chemical ordering in CoPt nanoalloys, *Faraday Discuss.* **138**, 193 (2008).
- [31] B. Legrand, M. Guillopé, J. S. Luo, and G. Tréglia, Multilayer relaxation and reconstruction in bcc and fcc transition and noble metals, *Vacuum* **41**, 311 (1990).
- [32] V. Rosato, M. Guillope, and B. Legrand, Thermodynamical and structural properties of f.c.c. transition metals using a simple tight-binding model, *Philos. Mag. A* **59**, 321 (1989).
- [33] F. Ducastelle, Modules élastiques des métaux de transition, *J. Phys. (Paris)* **31**, 1055 (1970).
- [34] C. Goyhenex, H. Bulou, J.-P. Deville, and G. Tréglia, Pt/Co(0001) superstructures in the submonolayer range: A tight-binding quenched-molecular-dynamics study, *Phys. Rev. B* **60**, 2781 (1999).
- [35] N. Levanov, V. Stepanyuk, W. Hergert, O. Trushin, and K. Kokko, Molecular dynamics simulation of Co thin films growth on Cu(001), *Surf. Sci.* **400**, 54 (1998).
- [36] D. E. Goldberg, *Genetic Algorithms in Search, Optimization and Machine Learning*, 1st ed. (Addison-Wesley-Longman, Boston, 1989).
- [37] J. F. Ziegler, U. Littmark, and J. P. Biersack, *The Stopping and Range of Ions in Solids* (Pergamon, New York, 1985).
- [38] H. J. C. Berendsen, J. P. M. Postma, W. F. van Gunsteren, A. DiNola, and J. R. Haak, Molecular dynamics with coupling to external bath, *J. Chem. Phys.* **81**, 3684 (1984).
- [39] J. F. Ziegler, M. D. Ziegler, and J. P. Biersack, SRIM - The stopping and range of ions in matter (2010), *Nucl. Instrum. Methods Phys. Res., Sect. B* **268**, 1818 (2010).
- [40] R. W. Siegel, Vacancy concentrations in metals, *J. Nucl. Mater.* **69–70**, 117 (1978).
- [41] A. Stukowski, Structure identification methods for atomistic simulations of crystalline materials, *Modell. Simul. Mater. Sci. Eng.* **20**, 045021 (2012).
- [42] J. D. Honeycutt and H. C. Andersen, Molecular dynamics study of melting and freezing of small Lennard-Jones clusters, *J. Phys. Chem.* **91**, 4950 (1987).
- [43] A. Stukowski, Visualization and analysis of atomistic simulation data with OVITO - the Open Visualization Tool, *Modell. Simul. Mater. Sci. Eng.* **18**, 015012 (2010).
- [44] A. Stukowski, Computational analysis methods in atomistic modeling of crystals, *JOM* **66**, 399 (2014).
- [45] B. Sadigh, P. Erhart, A. Stukowski, A. Caro, E. Martinez, and L. Zepeda-Ruiz, Scalable parallel Monte Carlo algorithm for atomistic simulations of precipitation in alloys, *Phys. Rev. B* **85**, 184203 (2012).
- [46] W. Möller and W. Eckstein, TRIDYN - a TRIM simulation code including dynamic composition changes, *Nucl. Instrum. Methods Phys. Res., Sect. B* **2**, 814 (1984).
- [47] K. Nordlund, J. Keinonen, M. Ghaly, and R. S. Averback, Coherent displacement of atoms during ion irradiation, *Nature (London)* **398**, 49 (1999).
- [48] K. Nordlund, M. Ghaly, and R. S. Averback, Mechanisms of ion beam mixing in metals and semiconductors, *J. Appl. Phys.* **83**, 1238–1246 (1998).
- [49] M. Ghaly and R. S. Averback, Effect of Viscous Flow on Ion Damage Near Solid Surfaces, *Phys. Rev. Lett.* **72**, 364 (1994).
- [50] E. M. Bringa, K. Nordlund, and J. Keinonen, Cratering-energy regimes: from linear collision cascades to heat spikes to macroscopic impacts, *Phys. Rev. B* **64**, 235426 (2001).
- [51] K. Nordlund, J. Tarus, J. Keinonen, S. E. Donnelly, and R. C. Birtcher, Atomic fingers, bridges and slingshots: formation of exotic surface structures during ion irradiation of heavy metals, *Nucl. Instrum. Methods Phys. Res., Sect. B* **206**, 189 (2003).
- [52] G. Greaves, J. A. Hinks, P. Busby, N. J. Mellors, A. Ilinov, A. Kuronen, K. Nordlund, and S. E. Donnelly, Giant Sputtering Yields From Single-Ion Impacts on Gold Nanorods, *Phys. Rev. Lett.* **111**, 065504 (2013).
- [53] S. E. Donnelly and R. C. Birtcher, Heavy ion cratering of gold, *Phys. Rev. B* **56**, 13599 (1997).
- [54] K. O. E. Henriksson, K. Nordlund, and J. Keinonen, Crater annihilation on silver by cluster ion impacts, *Nucl. Instrum. Methods Phys. Res., Sect. B* **255**, 259 (2007).
- [55] J. Wang, J.-M. Albina, T. Iwasaki, H. Moriya, and Y. Umeno, Influence of normal and shear strain on magnetic anisotropy energy of hcp cobalt: An ab initio study, *J. Mater. Res.* **28**, 1559 (2013).
- [56] T. Diaz de la Rubia, A. Caro, and M. Spaczer, Kinetics of radiation-induced disordering of A_3B intermetallic compounds: A molecular-dynamics-simulation study, *Phys. Rev. B* **47**, 11483 (1993).
- [57] M. Spaczer, A. Caro, M. Victoria, and T. Diaz de la Rubia, Computer simulations of disordering kinetics in irradiated intermetallic compounds, *Phys. Rev. B* **50**, 13204 (1994).
- [58] J. Ye and P. Bellon, Nanoscale patterning of chemical order induced by displacement cascades in irradiated alloys. I. A kinetic Monte Carlo study, *Phys. Rev. B* **70**, 094104 (2004).
- [59] J. Ye and P. Bellon, Nanoscale patterning of chemical order induced by displacement cascades in irradiated $L1_0$ alloys: Scaling analysis of the fluctuations of order, *Phys. Rev. B* **73**, 224121 (2006).
- [60] K. Nordlund, M. Ghaly, R. S. Averback, M. Caturla, T. Diaz de la Rubia, and J. Tarus, Defect production in collision cascades in elemental semiconductors and fcc metals, *Phys. Rev. B* **57**, 7556 (1998).
- [61] M. Ghaly, K. Nordlund, and R. S. Averback, Molecular dynamics investigations of surface damage produced by keV self-bombardment of solids, *Philos. Mag. A* **79**, 795 (1999).
- [62] K. Nordlund, Molecular dynamics simulation of ion ranges in the 1–100 keV energy range, *Comput. Mater. Sci.* **3**, 448 (1995).